Journal of Power Sources 233 (2013) 313–319

Contents lists available at SciVerse ScienceDirect

Journal of Power Sources

journal homepage: www.elsevier.com/locate/jpowsour

Effect of pH-induced chemical modification of hydrothermally reduced graphene oxide on supercapacitor performance

Yaocai Bai, R.B. Rakhi, Wei Chen, H.N. Alshareef*

Materials science and Engineering, King Abdullah University of Science and Technology (KAUST), Thuwal 23955-6900, Saudi Arabia

HIGHLIGHTS

- Synthesis of reduced graphene oxide (rGO) by hydrothermal reduction of graphite oxide.
- Influence of pH value on the morphology and supercapacitor performance of rGOs.
- rGOs prepared under acidic condition exhibit a maximum specific capacitance of 225 F g^{-1}
- Functional groups present in the acidic sample induce additional pseudocapacitance effect.
- rGOs prepared under basic condition exhibit superior cycling stability.

GRAPHICAL ABSTRACT

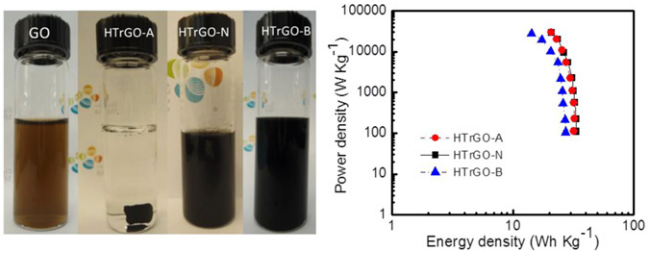

ARTICLE INFO

Article history:
Received 29 September 2012
Received in revised form
16 January 2013
Accepted 18 January 2013
Available online 29 January 2013

Keywords:
Supercapacitor
Graphene
pH
Specific capacitance
Hydrothermal
functionalization

ABSTRACT

Three kinds of reduced graphene oxides are prepared by hydrothermal reduction under different pH conditions and their pseudocapacitive performances are evaluated using full-cell supercapacitor devices. The pH values are found to have great influence on the performance of the supercapacitors, achieving the highest specific capacitance value reported for hydrothermal reduced graphene oxide supercapacitors. Acidic and neutral media yield reduced graphene oxides with more oxygen-functional groups and lower surface areas but with broader pore size distributions than those in basic medium. The graphene produced in the basic solution (nitrogen-doped graphene) presents mainly electrochemical double layer (ECDL) behavior with specific capacitance of 185 F g^{-1}, while the graphene produced under neutral or acidic conditions show both ECDL and pseudocapacitive behavior with specific capacitance of 225 F g^{-1} (acidic) and 230 F g^{-1} (neutral), respectively, at a constant current density of 1 A g^{-1}. The influence of pH on cycling performance and electrochemical impedance of the supercapacitive devices is also presented.

1. Introduction

Exasperating energy and environmental problems like global warming and depletion of fossil fuels create urgent demand for renewable energy production and efficient energy storage in modern society [1]. Supercapacitors are considered as one of the most promising electrochemical energy storage devices of the present century [2–4]. They have higher power densities and exceptional long cycle life than conventional batteries and higher energy densities than conventional dielectric capacitors. Based on charge storage mechanisms, supercapacitors are broadly classified into two categories viz, electrochemical double-layer capacitors

* Corresponding author. Tel.: +966 (0)2 808 4477, +966 (0)5 44700037 (mobile).
E-mail address: husam.alshareef@kaust.edu.sa (H.N. Alshareef).

0378-7753/$ – see front matter © 2013 Elsevier B.V. All rights reserved.
http://dx.doi.org/10.1016/j.jpowsour.2013.01.122

(EDLCs) and pseudocapacitors [5,6]. While in EDLCs, energy storage takes place by ion adsorption between electrode–electrolyte interface, pseudocapacitors store energy by fast and reversible Faradic reactions. Carbon based materials such as activated carbon, mesoporous carbon and graphitic nanocarbons (nanocoils, nanofibers, nanotubes, nanocones, etc) are widely used as electrode materials for EDLCs [7,8]. Commonly used electrode materials for pseudocapacitors are transition metal oxides and conducting polymers [5,9].

Graphene or reduced graphene oxide (rGO), a new class of 2-dimensional carbon nanostructure, has recently emerged as an outstanding candidate for supercapacitor electrode material because of its characteristics of chemical stability, high electrical conductivity, thermal stability, large surface area and broad electrochemical window [10–14]. Moreover, rGO can be prepared in large scale at low cost [15,16]. Various reports are available on the reduction of graphene oxide by different methods and the supercapacitor performances of rGO vary considerably in each case. Stoller et al. reported a specific capacitance of 135 F g^{-1} at a discharge current of 10 mA for chemically modified graphene prepared by hydrazine reduction of the graphite oxide solution [17]. Vivekchand et al. treated graphite oxide by thermal exfoliation at 1050 °C to obtain graphene with a specific capacitance of 117 F g^{-1} in 1 mol L^{-1} H_2SO_4 electrolyte [18]. Wang et al. prepared the graphene materials from gas-based hydrazine reduction which showed a specific capacitance of 205 F g^{-1} in aqueous electrolyte at a constant current density of 100 mA g^{-1} [19]. However, the facts that hydrazine is toxic and dangerously unstable and that the high temperature exfoliation process is energy-consuming, limit the application of those reduction methods [20].

Recently, Zhou et al. reported a simple, clean and controlled hydrothermal dehydration route to convert graphite oxide or graphene oxide (GO) to graphene [20]. Xu et al. fabricated the graphene hydrogel by hydrothermal method via increasing the GO concentration and applied it in supercapacitors [21]. In a recent work, Navarro et al. reported the important role played by the pH on the morphology and structure of the reduced graphene oxide (rGO) samples obtained by hydrothermal treatment of the previously prepared GO [22]. They demonstrated that reduction under acidic conditions lead to a higher amount of defects in the resulting rGO samples, with smaller sizes of the sheets, and a pronounced tendency of these sheets to aggregate giving rise to other graphitic nanoforms while more basic conditions promotes a decrease in the number of defects present in the resulting rGO and bigger graphitic domains. However, to the best of our knowledge, no reports are available on the effects of pH of the hydrothermal reaction solution on the supercapacitor properties of rGO. Herein, we report on the effect of specific pH values used in the synthesis of hydrothermally reduced graphene oxides on electrochemical properties, energy density, and cycling performance of full-cell supercapacitor devices.

2. Experimental methods

2.1. Preparation of graphite oxide

Graphite oxide was prepared by a modified Hummers' method [23,24]. Typically, 75 mL of concentrated sulfuric acid was added to 1.5 g of graphite powder and 1.5 g of sodium nitrate in a beaker and stirred for 15 min at room temperature before the beaker was kept in an ice bath. Then, 9 g of potassium permanganate was added slowly into the mixture and kept for 30 min. After the ice bath was removed, the reaction was continued for 48 h under stirring at room temperature. The resulting brown slurry or thick paste was then added into 138 mL of DI water and the suspension was stirred for 10 min. 420 mL of warm water was added followed by a slow addition of 30 mL of hydrogen peroxide to get a yellow suspension. The suspension was centrifuged and washed by a mixed aqueous solution of 6 wt% H_2SO_4/1 wt% H_2O_2, and then by water and dried in vacuum at 60 °C for 36 h to obtain the graphite oxide powder.

2.2. Reduction of graphite oxide

The graphite oxide was reduced by hydrothermal dehydration as reported with some modification [20]. Briefly, 37.5 mL of 0.5 mg mL^{-1} GO aqueous solution prepared by probe ultrasonication (160 W) for 1 h was sealed in a 50 mL teflon-lined autoclave and maintained at 180 °C for 6 h. It was then cooled to room temperature; the resultant black product was filtered and washed using DI water. The pH of the solution was adjusted with hydrochloric acid and ammonia solution, and the products were labeled as HTrGO-N (neutral, pH ~ 7), HTrGO-A (acidic, pH ~ 2), and HTrGO-B (basic, pH ~ 10).

2.3. General characterization

Powder X-ray diffraction studies were carried out using a Bruker D8 ADVANCE X-ray diffractometer with Cu K_α radiation (λ = 0.15406 nm) as the X-ray source. Raman spectroscopy was performed on Horiba LabRAM HR Raman Microscope with 532 nm laser excitation. Brunauer–Emmett–Teller (BET) surface areas were determined with a Micromeritics ASAP 2420 system using nitrogen as adsorptive at 77 K. Before measurements, the samples were degassed in vacuum at 200 °C for 12 h. Surface chemistry information was collected by X-ray photoelectron spectroscopy (XPS). Field

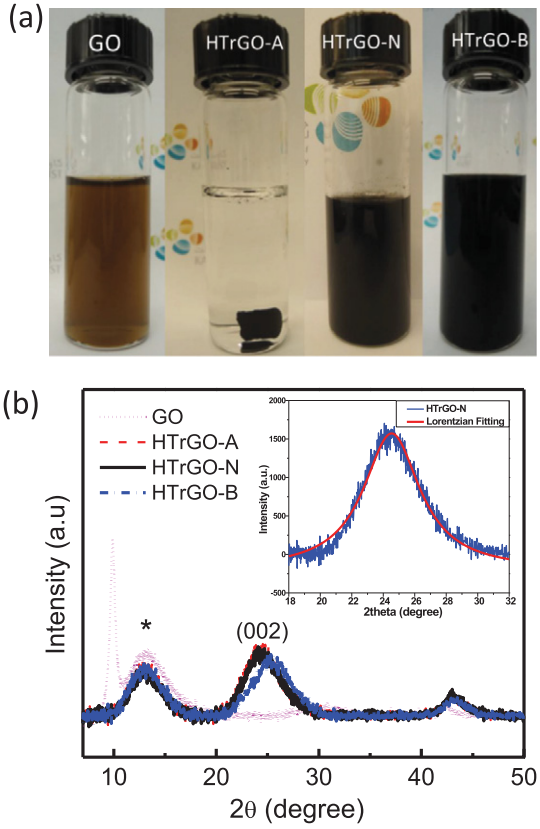

Fig. 1. (a) Photographs of GO solution and HTrGOs after hydrothermal treatment and (b) XRD patterns of GO and HTrGOs, the * peak comes from the sample holder. Inset shows the Lorentzian fitting of the (002) peak of HTrGO-N.

Table 1
Interlayer spacing, average number of graphene layers, specific area, C/O atomic ratio, and specific capacitance of HTrGOs.

Samples	d(002) spacing (Å)	No. of layers (calculated)	BET surface area ($m^2\ g^{-1}$)	C(1s)/O(1s) atomic ratio	C_{sp} (F g^{-1}) at 1 A g^{-1}
HTrGO-A	3.64	5.38	265.20	4.78	225
HTrGO-N	3.63	5.09	342.90	5.05	230
HTrGO-B	3.47	4.75	479.55	8.19	185

emission scanning electron microscopy (FEI Helios Nanolab) and transmission electron microscopy (FEI Titan) were used to investigate the morphology and microstructure of the samples.

2.4. Fabrication of the supercapacitors and electrochemical testing

Circular supercapacitor electrodes of 1.6 cm diameter were prepared using HTrGO samples by the following procedure. The HTrGos were mixed with polytetrafluoroethylene (PTFE) binder in a mass ratio of 95:5 and dispersed in ethanol. The resulting mixture was homogenized by ultrasonication and coated onto the conductive carbon paper substrate, which was followed by drying at 100 °C for 6 h in a vacuum oven. Each electrode contained 2.5 mg of electroactive material of electroactive material. The resultant mass loading was 1.25 mg cm^{-2}. The two electrodes were assembled into a coin cell separated by a thin polymer separator (Celgard® 3501) in 30 wt% KOH aqueous electrolyte. The electrochemical properties of the coin cell supercapacitors were studied by cyclic voltammetry (CV), galvanostatic charge/discharge and electrochemical impedance spectroscopy (EIS) using an electrochemical workstation (Model 660D, CH Instruments). The two electrode configuration is preferred as it provides the most reliable results of performance of a material for electrochemical capacitors. The EIS was performed in the frequency range from 100 kHz to 10 mHz at a 5 mV amplitude referring to open circuit voltage. The capacitance of carbon paper substrate can be neglected [25].

The cell capacitance (C in F) was then calculated from the charge–discharge curves according to Eq. (1)

$$C = \frac{I}{(\Delta V/\Delta t)} \tag{1}$$

where 'I' is the constant current for charge–discharge, $\Delta V/\Delta t$ is slope of the discharge curve [26]. The specific capacitance (C_{sp}in F g^{-1}) was then calculated as

$$C_{sp} = \frac{2C}{m} \tag{2}$$

where 'm' is the mass of electroactive material in each electrode.

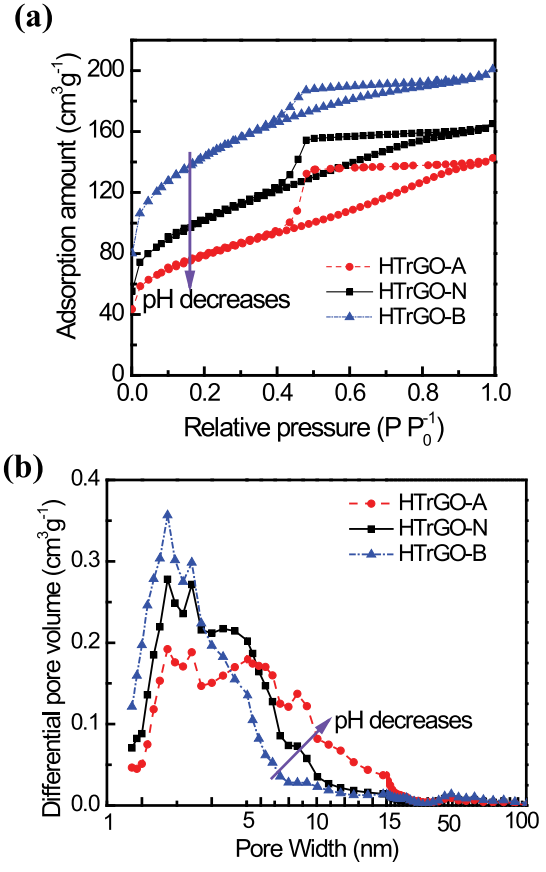

Fig. 2. (a) N_2 adsorption–desorption isotherms of HTrGOs and (b) BJH pore size distributions.

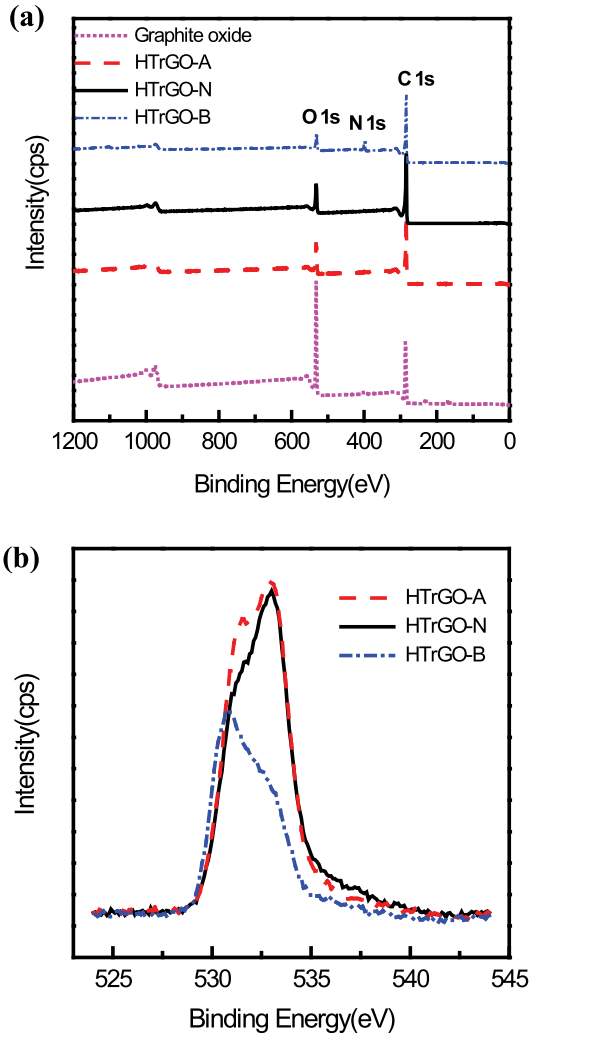

Fig. 3. (a) XPS spectra of graphite oxide and HTrGOs and (b) O 1s spectra of HTrGOs.

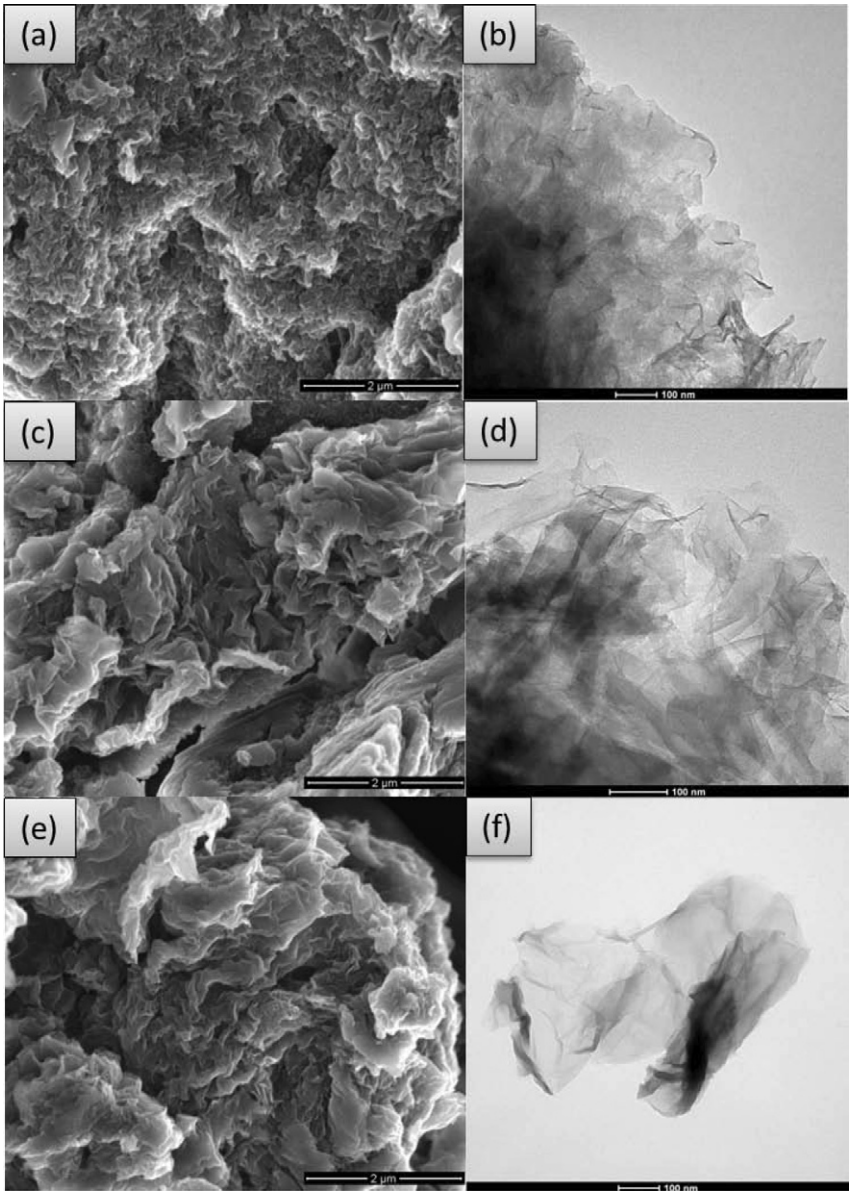

Fig. 4. SEM and TEM images of (a, b) HTrGO-A, (c, d) HTrGO-N, and (e, f) HTrGO-B.

The energy (E) and power (P) densities were calculated from charge–discharge curves at different current densities using Eq. (3) and Eq. (4) respectively

$$E = \frac{1}{2} C_{sp} \Delta V^2 \tag{3}$$

where 'ΔV' is the potential window of discharge process.

$$P = \frac{E}{\Delta t} \tag{4}$$

where 'Δt' is the discharge time.

3. Results and discussion

As shown in Fig. 1(a), the HTrGOs were produced in different forms after hydrothermal treatment, depending on the pH of the solution. The acidic solution yielded aggregated graphene or graphene hydrogel while neutral and basic solutions resulted in stable graphene solutions. The reduction mechanism is likely related to H^+ catalyzed intramolecular and intermolecular dehydration [20]. The small magnitude of the negative zeta potential of the GO solution in acidic media leads to the intermolecular dehydration to form aggregated graphene via ether linkages [20,27,28]. Fig. 1(b) shows the powder XRD patterns of graphite oxide, HTrGO-A, HTrGO-N, and HTrGO-B. Due to the insertion of oxygenated groups and H_2O molecules, the (002) diffraction peak of GO appears at $2\theta = 9.90°$, with an enlarged interlayer spacing of 8.93 Å. The (002) reflections from HTrGO-A, HTrGO-N, and HTrGO-B shift to higher 2θ values 24.43°, 24.49° and 24.65° respectively, indicating decrease in interlayer spacing of rGOs with increase in pH values. The interlayer spacing of HTrGO-B (3.47 Å) is smaller than the other two, but still larger than graphite (3.41 Å), suggesting fewer residual oxygenated groups or functional groups in HTrGO-B [29]. Analysis of these broad peaks indicates the poor order and

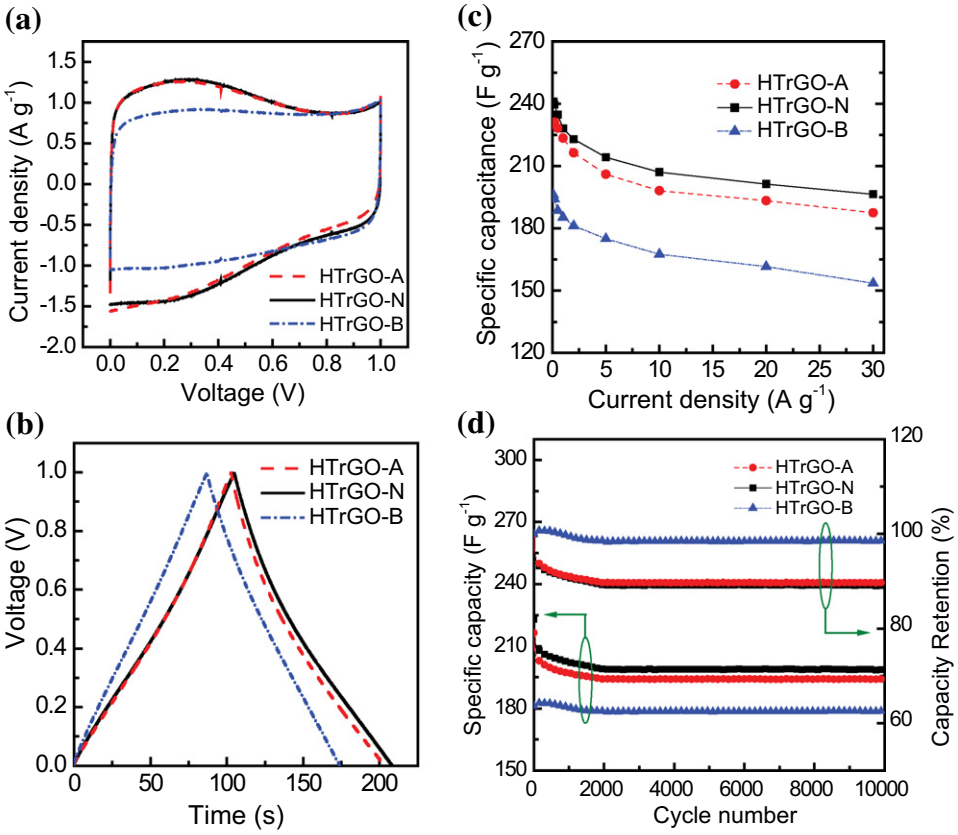

Fig. 5. (a) Cyclic voltammograms for HTrGOs at scan rate of 10 mV s^{-1}; (b) Galvanostatic charge–discharge curve for HTrGOs at a constant current density of 1 A g^{-1}; (c) Specific capacitance of HTrGOs at different current densities; (d) Cycling performance (10,000 charge–discharge cycles at a constant current density of 2 A g^{-1}).

multilayer character of graphene sheets. Through Lorentzian fitting and Debye–Scherrer equation, the average number of stacked graphene sheets is calculated to be four to six layers [30,31] (see Table 1). The number of layers was found to decrease with the increase of pH value of the reaction solution. Raman spectra (see ESI) show very small increase in the I_D/I_G ratios from 0.94 (GO) to ~1.05 (HTrGO) indicating good defect repairs [20], and very small differences among the HTrGOs.

The nitrogen adsorption and desorption isotherms and pore size distributions for rGO under the three different pH conditions are shown in Fig. 2. The BET surface areas of HTrGO-A, HTrGO-N, and HTrGO-B are 265.20, 342.90, and 479.55 m^2 g^{-1} respectively. The minimum surface area obtained for the acidic sample is consistent with the agglomeration of rGOs at lower pH. All the isotherms are characterized as type IV with hysteresis loops in the relative pressure region between 0.4 and 1.0 according to the International Union of Pure and Applied Chemistry (IUPAC) classification [15,32,33], indicating the mesoporous structures as shown in the pore size distributions obtained by means of Barret–Joyner–Halenda (BJH) equation. The intermolecular dehydration in acidic solution will yield broader pore size distributions because the graphene sheets will connect each other via ether linkages which will likely introduce larger pores.

The XPS survey spectra for HTrGOs are shown in Fig. 3(a). The decrease in the intensity of O 1s peak after hydrothermal reaction, indicates the deoxygenation or reduction process. Atomic ratios of carbon to oxygen for HTrGO-A, HTrGO-N and HTrGO-B samples are calculated as 4.78, 5.05, and 8.19 respectively, indicating minimum amount of oxygenated groups for HTrGO-B. Nitrogen incorporated into the rGOs in ammonia tuned basic media explains the good dispersion capability of HTrGO-B by virtue of the increased numbers of hydrophilic polar sites [34]. Due to the smaller O 1s sampling depth, the O 1s spectra are more surface specific [35]. High resolution O 1s spectra for the rGOs are shown in Fig. 3(b) which can be used to compare the surface chemistry of the HTrGOs. There are mainly two peaks located at 530–532 eV and ~533 eV respectively. The former peak is attributed to C=O type oxygen (carbonyl, –COOR in ester) while the latter one is related to the C–O–C type oxygen (in ether) or C–OH groups (in carboxyl or hydroxyl group) [35–38]. The peak of O 1s spectra of HTrGO-B is weaker than that of HTrGO-A and HTrGO-N, indicating better reduction efficiency. There are relatively more C=O type oxygen than C–O–C or C–OH type oxygen in HTrGO-B due to the removal of C–OH by intramolecular dehydration [20].

Fig. 4 shows the representative SEM and TEM images of HTrGOs. The SEM images indicate that all HTrGOs form dense agglomerates with layered structure in dry state and the nanosheets exhibit curved/wrinkled morphology. The curved morphology prevents the graphene sheets from restacking among one another and contributes to the mesoporous nature [14], The mesopores and wrinkles on the surface of graphene sheets may shorten the ion diffusion lengths in supercapacitors and ensure the full utilization of the graphene nanosheets with improved transport of electrolyte ions [33]. The TEM images also show multilayer graphene sheets with wrinkled structures.

Fig. 5(a) shows the CV curves of HTrGOs in a potential range of 0–1 V at a scan rate of 10 mV s^{-1}. Due to different degrees of reduction of GO, the shapes of the CV curves vary. HTrGO-B shows better EDLC characteristic with lower capacity while the other two present additional pseudocapacitance with higher capacity. Supercapacitors using HTrGO-A and HTrGO-N exhibit very similar CV behaviors and specific capacitance (C_{sp}), due to the

presence of functional groups attached to graphene sheets [38,39]. The functional groups such as hydroxyl, carboxyl and epoxy groups result in fast redox processes in HTrGO-A and HTrGO-B, resulting in additional pseudocapacitive contribution along with the EDLC behavior giving rise to larger C_{sp} values [39]. A broad peak at ~0.3 V for CV curves of HTrGO-A and HTrGO-N is observed, which could be attributed to the oxygen-related functionalities [39]. The quasi-rectangular shapes can be well kept with less distortion even at higher scan rate of 300 mV s^{-1} (see ESI) indicating low resistance. Unlike the HTrGO-A and HTrGO-N electrodes, CV loop of nitrogen-doped graphene (HTrGO-B) retains nearly rectangular shape indicating ideal double-layer capacitive behavior without any pseudocapacitive contribution to its overall capacitance. Hence its overall capacitance is lower than that of the other two samples.

The galvanostatic charge/discharge curves for HTrGOs at the current density of 1 A g^{-1} in the potential range of 0 to +1 V are shown in Fig. 5(b). The specific capacitance at current density of 1 A g^{-1} for HTrGO-A, HTrGO-N and HTrGO-B are 225, 230 and 185 F g^{-1} respectively. This result shows that the pH can induce nearly 24% difference in the specific capacitance of supercapacitor devices that use HTrGOs. The result also shows one of the highest specific capacitance reported for the rGO. The specific capacitance values obtained for HTrGO-A and HTrGO-N based supercapacitors in the present study are better than those reported by Stroller et al. [17] and by Wang et al. [19]. The values are comparable to those reported by Zhang et al. for rGO prepared by a combination method of hydrothermal dehydration and hydrazine reduction (222 F g^{-1} at 1 A g^{-1}) [40]. Considering that three-electrode configuration yields higher specific capacitance values than in the two-electrode measurements [41], the specific capacitance values obtained for HTrGO-A and HTrGO-N are better than those reported by Lin et al. (276 F g^{-1} at 0.1 A g^{-1}) [42], by Yan et al. (227 F g^{-1} at 1 A g^{-1}) [33], and by Zhao et al. (260.5 F g^{-1} at 0.4 A g^{-1}) [43]. Inspite of its large BET surface area value, nitrogen-doped HTrGO-B shows lower specific capacitance than the acidic and neutral samples. It is clear that the surface functionalization of graphene induced by pH control plays an important role on the performance of supercapacitors. Even then the C_{sp} value obtained for HTrGO-B is still higher than that reported by Sun et al. (326 F g^{-1} at 0.2 A g^{-1} in three electrode configuration) [44].

Variations in specific capacitance values with increase in current density for the three supercapacitors are shown in Fig. 5(c). The figure indicates that all the HTrGOs show good rate performance; where over 83% of the initial capacitance (1 A g^{-1}) was retained at high current density of 30 A g^{-1}. In general, at current densities lower than 5 A g^{-1}, the specific capacitance decreases with the increase in discharge current density and above 5 A g^{-1} specific capacitance tends to stabilize. The rate performance of HTrGOs used in the present study is superior to that reported by Lin et al. (74% of the initial capacitance was retained at a current density of 5 A g^{-1}) or by Zhao et al. (68% of the initial capacitance was retained at a high current density of 20 A g^{-1}) [42,43]. Zhang et al. conducted rate performance studies over a current density range of 1–100 A g^{-1}. Within a current density range of 1–30 A g^{-1}, the results obtained in the present study are comparable to that reported by Zhang and Shi [40].

The cycle life, which is a key evaluation factor for practical applications of supercapacitors [2], was measured by galvanostatic charge–discharge technique between 0 and +1 V at a current density of 2 A g^{-1} for 10,000 cycles. HTrGO-B based supercapacitor exhibited excellent capacitance retention of ~98% after 10,000 cycles. Capacitance retention for the other two HTrGOs is ~89%. Those good capacity retentions suggest the HTrGOs hold good stability and high degree of reversibility in the repetitive charge–discharge cycling [19]. For HTrGO-A and HTrGO-N based capacitors, the capacitance losses occur mainly in the first hundred cycles

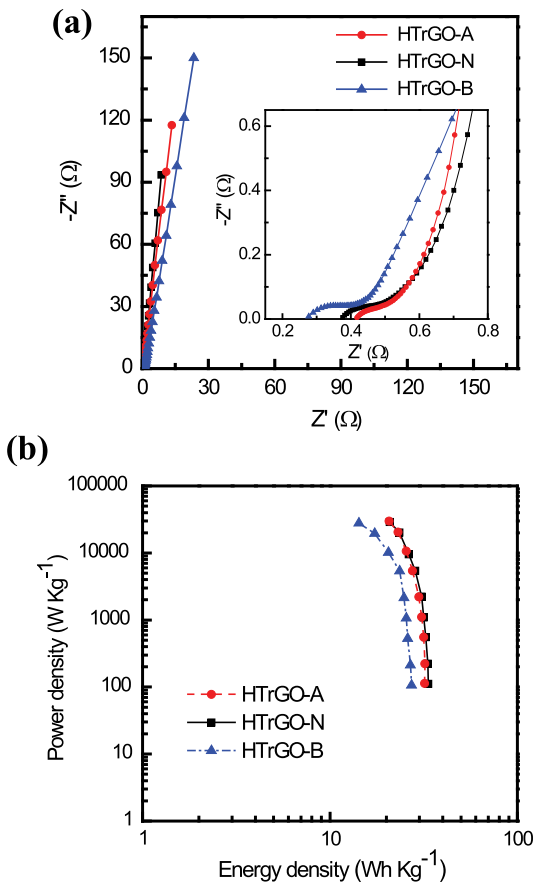

Fig. 6. (a) Nyquist plots and (b) Ragone plot for supercapacitors based on HTrGOs.

(loss of nearly 6% of the initial capacitance after 100 cycles) and they became quite stable after that. This is due to the removal of some functional groups and disappearance of some of the pseudocapacitance during the first hundred cycles [39].

The EIS data in the form of Nyquist plots (Fig. 6(a)) show that all HTrGOs display inconspicuous arcs in the high frequency region and straight lines in the low frequency region. The high frequency loop is related to electronic resistance and all HTrGOs show very small electronic resistance (~0.15 Ω). The magnitude of equivalent series resistance (ESR) is obtained from the *x*-intercept and all HTrGOs show small ESR (~0.4 Ω), indicating excellent power density of the HTrGOs based supercapacitors. The vertical shape at lower frequencies indicates a pure capacitive behavior and represents ion diffusion in the structure of electrode. The straight lines of HTrGO-A and HTrGO-N are steeper than that of HTrGO-B, indicating faster ion movement and closer behavior to ideal capacitors. Fig. 6(b) shows the Ragone plot (power density vs. energy density) of the symmetric supercapacitors based on HTrGOs. At a constant power density of 20 kW kg^{-1}, the energy density obtained for HTrGO-B is 17.1 Wh kg^{-1} while both HTrGO-N and HTrGO-A show higher energy densities of ~23.5 Wh kg^{-1}. These results indicate that HTrGO-N and HTrGO-A are very promising electrode materials for high performance supercapacitors.

4. Conclusions

In conclusion, we prepared rGOs by hydrothermal reduction under different pH conditions and found that pH plays an important role in controlling the properties of the resultant supercapacitor performance. While HTrGO-A and HTrGO-N displayed

both EDLC and pseudocapacitance effects with very high specific capacities (~230 F g^{-1} at 1 A g^{-1}), HTrGO-B exhibited mostly EDLC behavior with lower specific capacity.

Acknowledgments

Authors acknowledge the help from Dr M. N. Hedhili, (research scientist, Advanced Nanofabrication, Imaging & Characterization Lab, KAUST) for the XPS measurements and the help from Analytical Chemistry Core Lab (KAUST) in BET measurements. R.B.R. acknowledges the financial support from SABIC Post Doctoral Fellowship. W.C. acknowledges support from KAUST Graduate Fellowship. H.N.A. acknowledges the generous support from the KAUST baseline fund.

Appendix A. Supplementary data

Supplementary data related to this article can be found at http://dx.doi.org/10.1016/j.jpowsour.2013.01.122.

References

[1] M.A. Guerrero, E. Romero, F. Barrero, M.I. Milanes, E. Gonzalez, Przeglad Elektrotechniczny 85 (2009) 188–195.
[2] B.E. Conway, Electrochemical Supercapacitors: Scientific Fundamentals and Technological Applications, Kluwer Academic/Plenum, New York, 1999.
[3] R. Kotz, M. Carlen, Electrochim. Acta 45 (2000) 2483–2498.
[4] M. Conte, Fuel Cells 10 (2010) 806–818.
[5] Y. Zhang, H. Feng, X.B. Wu, L.Z. Wang, A.Q. Zhang, T.C. Xia, H.C. Dong, X.F. Li, L.S. Zhang, Int. J. Hydrogen Energy 34 (2009) 4889–4899.
[6] R.B. Rakhi, W. Chen, H.N. Alshareef, J. Mater. Chem. 22 (2012) 5177–5183.
[7] M. Inagaki, H. Konno, O. Tanaike, J. Power Sources 195 (2010) 7880–7903.
[8] A.G. Pandolfo, A.F. Hollenkamp, J. Power Sources 157 (2006) 11–27.
[9] G.M. Jacob, Q.M. Yang, I. Zhitomirsky, J. Appl. Electrochem. 39 (2009) 2579–2585.
[10] A.K. Geim, K.S. Novoselov, Nat. Mater. 6 (2007) 183–191.
[11] H.A. Becerril, J. Mao, Z. Liu, R.M. Stoltenberg, Z. Bao, Y. Chen, ACS Nano 2 (2008) 463–470.
[12] S. Stankovich, D.A. Dikin, R.D. Piner, K.A. Kohlhaas, A. Kleinhammes, Y. Jia, Y. Wu, S.T. Nguyen, R.S. Ruoff, Carbon 45 (2007) 1558–1565.
[13] S. Park, R.S. Ruoff, Nat. Nanotechnol. 4 (2009) 217–224.
[14] C.G. Liu, Z.N. Yu, D. Neff, A. Zhamu, B.Z. Jang, Nano Lett. 10 (2010) 4863–4868.
[15] Y.W. Zhu, S. Murali, M.D. Stoller, K.J. Ganesh, W.W. Cai, P.J. Ferreira, A. Pirkle, R.M. Wallace, K.A. Cychosz, M. Thommes, D. Su, E.A. Stach, R.S. Ruoff, Science 332 (2011) 1537–1541.
[16] M. Segal, Nat. Nanotechnol. 4 (2009) 611–613.
[17] M.D. Stoller, S.J. Park, Y.W. Zhu, J.H. An, R.S. Ruoff, Nano Lett. 8 (2008) 3498–3502.
[18] S.R.C. Vivekchand, C.S. Rout, K.S. Subrahmanyam, A. Govindaraj, C.N.R. Rao, J. Chem. Sci. 120 (2008) 9–13.
[19] Y. Wang, Z.Q. Shi, Y. Huang, Y.F. Ma, C.Y. Wang, M.M. Chen, Y.S. Chen, J. Phys. Chem. C 113 (2009) 13103–13107.
[20] Y. Zhou, Q.L. Bao, L.A.L. Tang, Y.L. Zhong, K.P. Loh, Chem. Mater. 21 (2009) 2950–2956.
[21] Y.X. Xu, K.X. Sheng, C. Li, G.Q. Shi, ACS Nano 4 (2010) 4324–4330.
[22] C. Bosch-Navarro, E. Coronado, C. Marti-Gastaldo, J.F. Sanchez-Royo, M.G. Gomez, Nanoscale 4 (2012) 3977–3982.
[23] W.S. Hummers, R.E. Offeman, J. Am. Chem. Soc. 80 (1958) 1339.
[24] P.C. Lian, X.F. Zhu, S.Z. Liang, Z. Li, W.S. Yang, H.H. Wang, Electrochim. Acta 55 (2010) 3909–3914.
[25] R.B. Rakhi, W. Chen, D.K. Cha, H.N. Alshareef, J. Mater. Chem. 21 (2011) 16197–16204.
[26] V. Khomenko, E. Frackowiak, F. Beguin, Electrochim. Acta 50 (2005) 2499–2506.
[27] D. Li, M.B. Muller, S. Gilje, R.B. Kaner, G.G. Wallace, Nat. Nanotechnol. 3 (2008) 101–105.
[28] X.B. Fan, W.C. Peng, Y. Li, X.Y. Li, S.L. Wang, G.L. Zhang, F.B. Zhang, Adv. Mater. 20 (2008) 4490–4493.
[29] A.V. Murugan, T. Muraliganth, A. Manthiram, Chem. Mater. 21 (2009) 5004–5006.
[30] S.Y. Yang, K.H. Chang, H.W. Tien, Y.F. Lee, S.M. Li, Y.S. Wang, J.Y. Wang, C.C.M. Ma, C.C. Hu, J. Mater. Chem. 21 (2011) 2374–2380.
[31] K.S. Subrahmanyam, S.R.C. Vivekchand, A. Govindaraj, C.N.R. Rao, J. Mater. Chem. 18 (2008) 1517–1523.
[32] K.S.W. Sing, D.H. Everett, R.A.W. Haul, L. Moscou, R.A. Pierotti, J. Rouquerol, T. Siemieniewska, Pure Appl. Chem. 57 (1985) 603–619.
[33] J. Yan, J.P. Liu, Z.J. Fan, T. Wei, L.J. Zhang, Carbon 50 (2012) 2179–2188.
[34] D. Hulicova, M. Kodama, H. Hatori, Chem. Mater. 18 (2006) 2318–2326.
[35] D. Yang, A. Velamakanni, G. Bozoklu, S. Park, M. Stoller, R.D. Piner, S. Stankovich, I. Jung, D.A. Field, C.A. Ventrice, R.S. Ruoff, Carbon 47 (2009) 145–152.
[36] O. Akhavan, Carbon 48 (2010) 509–519.
[37] S.D. Gardner, C.S.K. Singamsetty, G.L. Booth, G.R. He, C.U. Pittman, Carbon 33 (1995) 587–595.
[38] W. Lv, D.M. Tang, Y.B. He, C.H. You, Z.Q. Shi, X.C. Chen, C.M. Chen, P.X. Hou, C. Liu, Q.H. Yang, ACS Nano 3 (2009) 3730–3736.
[39] Q.L. Du, M.B. Zheng, L.F. Zhang, Y.W. Wang, J.H. Chen, L.P. Xue, W.J. Dai, G.B. Ji, J.M. Cao, Electrochim. Acta 55 (2010) 3897–3903.
[40] L. Zhang, G.Q. Shi, J. Phys. Chem. C 115 (2011) 17206–17212.
[41] M.D. Stoller, R.S. Ruoff, Energy Environ. Sci. 3 (2010) 1294–1301.
[42] Z.Y. Lin, Y. Liu, Y.G. Yao, O.J. Hildreth, Z. Li, K. Moon, C.P. Wong, J. Phys. Chem. C 115 (2011) 7120–7125.
[43] B. Zhao, P. Liu, Y. Jiang, D.Y. Pan, H.H. Tao, J.S. Song, T. Fang, W.W. Xu, J. Power Sources 198 (2012) 423–427.
[44] L. Sun, L. Wang, C. Tian, T. Tan, Y. Xie, K. Shi, M. Li, H. Fu, RSC Adv. 2 (2012) 4498–4506.